



Structural, electrical and magnetic behaviour of undoped and nickel doped nanocrystalline bismuth ferrite by solution combustion route

Kakali Sarkar¹, Soumya Mukherjee^{2,*}, Siddhartha Mukherjee²

¹*School of Material Science & Nanotechnology, Jadavpur University, Kolkata-700032, India*

²*Department of Metallurgical & Material Engineering, Jadavpur University, Kolkata-700032, India*

Received 29 January 2015; Received in revised form 23 March 2015; Accepted 30 March 2015

Abstract

Multiferroic bismuth ferrite (BFO) and Ni-doped bismuth ferrites, with perovskite structure, were synthesized by chemical route at the temperatures ranging from 500 to 600 °C in controlled atmosphere. The structural phase analysis of materials was identified by XRD and crystallite size was calculated from the half width measurement of the well defined major XRD diffraction peak. Average crystallite size was calculated by applying Scherrer's formula and found to have values in the range from 14 to 35 nm. FESEM was used to evaluate the morphology and structural formation of nanocrystallite grains, while EDX confirmed elemental composition including the presence of dopant in the matrix. Dielectric properties and effect of electric field on polarization behaviour were studied for both undoped and Ni-doped BFO. Doping shows a clear change in ferroelectric behaviour. Antiferromagnetic nature of bulk bismuth ferrite transforms to superparamagnetic strong ferroelectric nature for both undoped and nickel doped nanocrystalline bismuth ferrite due to its close dimension of crystallite size with magnetic domains leading to break-down of frustrated spin cycloidal moment. The superparamagnetism behaviour is more pronounced for the nickel doped BFO though magnetic saturation is slightly higher for the undoped nanocrystalline bismuth ferrite.

Keywords: *Ni-doped bismuth ferrites, microstructure, dielectric, ferroelectric and magnetic properties*

I. Introduction

Multiferroics are class of materials which have coupled ferroelectricity, ferromagnetism or antiferromagnetic properties. An ideal multiferroic would be a ferroelectric and ferromagnetic exhibiting strong coupling between two order parameters at room temperature. Such a strong multiferroic system has not emerged yet; instead, there is a vibrant focus on antiferromagnetic ferroelectrics such as bulk BiFeO_3 (BFO) that can be coupled to ferromagnetic materials to achieve the desired coupling between electric fields and ferromagnetism at room temperature [1–5]. BFO is one of the most widely studied multiferroic materials over the last decade largely because it is the only single phase multiferroic material that simultaneously behaves both as antiferromagnetic and ferroelectric at room temperature (Neel temperature is $T_N = 643$ K and ferroelectric Curie temperature is $T_C = 1103$ K) [6,7], having rhom-

bohedrally distorted perovskite structure with $R3c$ space group at room temperature, exhibiting strong ferroelectricity and weak magnetism with spin cycloidal structure [8,9]. However, these two ordered parameters are mutually exclusive in principle because ferroelectricity and magnetism require different filled up states of d shells of transition metal ions. Empty d shells mainly exist in ferroelectricity, while partially filled d shells are required in magnetism. Therefore, multiferroics are rare and exhibit weak magnetism at room temperature. The rapid progress in radio, television, microwave and satellite communications, audio-video and digital recording along with focus on permanent magnets system has been creating a high demand for the development of multiferroic materials. BiFeO_3 structure or properties have been intensively studied [6,8–15], while its practical applications are hindered by the leakage current problems arising out of nonstoichiometry due to oxygen vacancy. This is mostly because of the difficulty in obtaining stoichiometric single phase BiFeO_3 materials as noted from study of $\text{Bi}_2\text{O}_3\text{-Fe}_2\text{O}_3$ phase

*Corresponding author: tel: +919830179414
e-mail: smmukherjee3@gmail.com

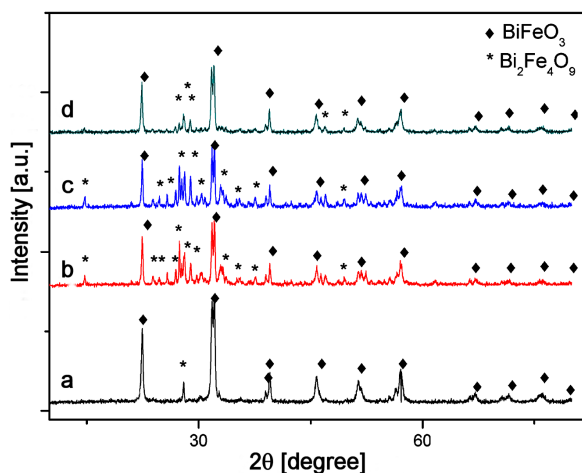


Figure 1. XRD of 5 mol% Ni-doped BFO samples heat treated at different temperatures: a) 500 °C-30 min, b) 550 °C-30 min, c) 600 °C-30 min and d) 600 °C-3 h

diagram an important step for thermodynamic stability of the perovskite bismuth ferrite. It is well-known that synthesizing the phase pure BiFeO_3 is difficult through the traditional solid-state sintering process [16]. The effect of nickel doping may create many interesting changes on the properties of nanocrystalline BFO because of defect structure which needs to be investigated. Moreover, Ni-doping will prevent leakage by putting constraints on oxygen vacancy generation. Thus, an attempt has been made to prepare phase pure BFO by wet synthesis technique and to observe the influence of Ni doping on the electrical and magnetic property of nanocrystalline BFO.

II. Experimental procedure

2.1. Synthesis

BFO and Ni-doped BFO were prepared by chemical route using precursor materials like bismuth nitrate [$\text{Bi}(\text{NO}_3)_3 \cdot 5\text{H}_2\text{O}$], ferric nitrate [$\text{Fe}(\text{NO}_3)_3 \cdot 9\text{H}_2\text{O}$], acetic acid, nickel acetate and ethylene glycol monoethyl ether. The solution was made of bismuth nitrate and ferric nitrate in 1:1 stoichiometric molar ratio, dissolved in the acetic acid and ethylene glycol monoethyl ether. Each precursor was dissolved in the respective solvent to form a solution under constant stirring at a

temperature of 45–50 °C for 45 minutes. After ensuring that there is no sedimentation/precipitation, both precursors were mixed together and kept at 70 °C under constant stirring for 1.5–3 h to homogenize mixing. Nickel acetate [$(\text{CH}_3\text{COO})_2\text{Ni} \cdot 4\text{H}_2\text{O}$] was used upto 3, 5 and 10 mol% to prepare Ni-doped BFO. After mixing the nickel acetate [$(\text{CH}_3\text{COO})_2\text{Ni} \cdot 4\text{H}_2\text{O}$] in the solution, it was stirred for 45 minutes at room temperature. The solution was subsequently heated to 60 °C for drying till (2–2.5 h) all liquids gets evaporated. The dried sample was heated up slowly at the heating rate of about 10 °C/min in N_2 (nitrogen) atmosphere to 300 °C to get calcined product. The calcined sample was then quickly raised to proper thermal treatment temperatures of 500, 550 and 600 °C for 30 minutes. The samples were leached using HNO_3 (15–20 drops) to remove impure phases and obtain the phase pure undoped BFO and nickel doped BFO material.

The prepared powders (using optimal quantity of about 2 g) were uniaxially pressed in steel die and mold, applying hydraulic pressure of 40 t/cm² for 1 minute. The pelletized samples were then sintered at the same conditions used for heat treatment of the as-synthesized powder samples. Densities of the sintered pellets were measured using Archimedes principle.

2.2. Characterization techniques

The structural analysis of phase formation was identified by X-ray diffraction (Rigaku Ultima III) using $\text{CuK}\alpha$ radiation ($\lambda = 0.154059\text{ nm}$) as a source in a continuous scan mode from 10° to 80° with scan rate maintained at 5°/min. The surface morphology and micro-structure formation were studied by field emission scanning electron microscope (FESEM) using Hitachi S4800 and for EDX analysis conducting coating of Pt-Rh was applied by sputtering under vacuum using JEOL JFC-1600 Auto Fine Coater. Elemental analysis of the synthesized material was carried out by EDX using INCAX-sight Oxford Instruments. Dielectric properties were measured with Hioki 3522-50 LCR Hi Tester for the undoped and Ni doped bismuth ferrite samples. Ferroelectric behaviour was measured with P - E loop tracer (Marine India Electrics, Ltd) while magnetic measurements were analysed by Physical Property Measurement System (PPMS, Cryogen, UK).

Table 1. Calculated crystallite size using Scherrer's formula of powders heat treated under different conditions

Sample composition	Heat treatment temperature [°C]	Duration of heat treatment [min]	Crystallite size [nm]
BFO	500	30	14.7
3% Ni Doped BFO	500	30	16.0
5% Ni Doped BFO	500	30	15.4
	550	30	34.5
	600	30	36.7
	600	180	39.1
10% Ni Doped BFO	500	30	16.5

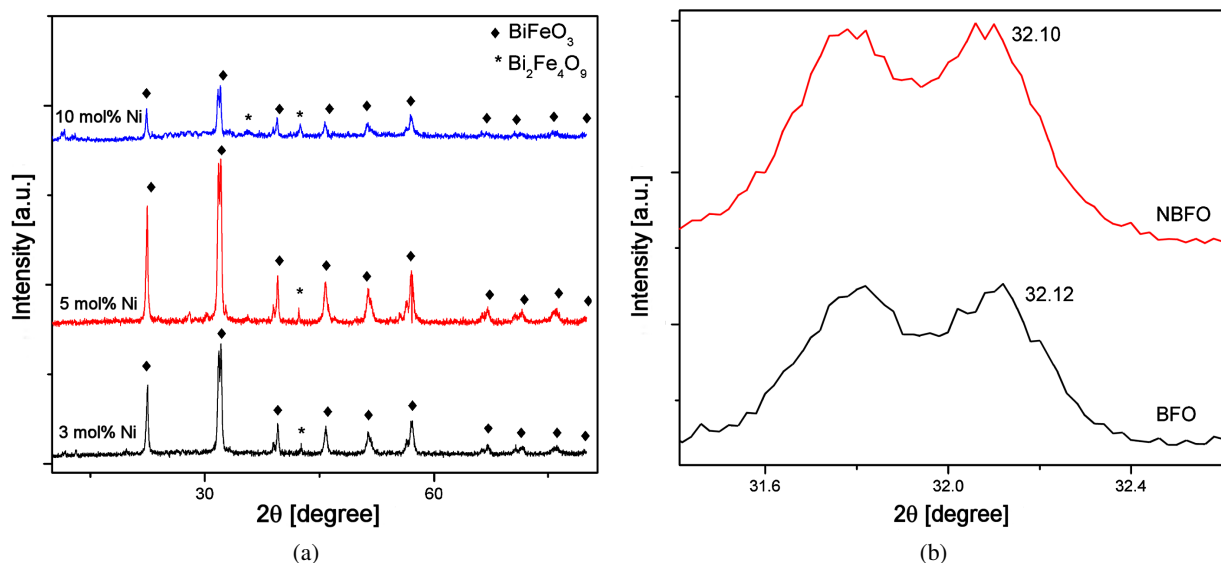


Figure 2. XRD patterns of samples heat treated at 500 °C for 30 min: a) BFO doped with 3, 5 and 10 mol% Ni and b) undoped (BFO) and 5 mol% Ni doped (NBFO) samples in selected 2θ range

III. Results and discussion

3.1. Phase analysis

Figure 1 shows the X-ray diffraction of Ni-doped BFO heat treated at 500 °C for 30 minutes (JCPDS card no. 74-2493). Diffraction peak corresponding to maximum intensity occurred can be seen at 32.12° (2θ) which matches with the pure phase of bismuth ferrites [17]. The average crystallite size was estimated by Scherrer's formula $t = 0.9\lambda/(\beta \cos \theta_B)$ (where t is crystallite size, β is half width full maxima, θ_B is angle between θ_1 and θ_2) from XRD data shown in Table 1. The crystallite size increases with increasing calcined temperature due to thermally activated diffusion.

Ni-doped BFO powders calcined at 500 °C exhibits a small amount of secondary $\text{Bi}_2\text{Fe}_4\text{O}_9$ phase, whereas XRD patterns of the samples heat treated at 550 and 600 °C have a few weak peaks of the secondary phase (Fig. 1). Thus, in subsequent experiments, annealing temperature was maintained at 500 °C to obtain the desired phase purity. The 3 mol% Ni-doped BFO annealed at 500 °C shows very weak peaks of the secondary $\text{Bi}_2\text{Fe}_4\text{O}_9$ phase. When concentration of dopant increases to the extent of 5 and 10 mol%, peaks of $\text{Bi}_2\text{Fe}_4\text{O}_9$ phase remain similar which are shown in Fig. 2a. However, the crystallite size for the sample with 5 mol% doping is found to be smaller than 3 and 10 mol% doping. The crystallite sizes of all samples are given in Table 1. The secondary phase does not induce any constraints to the properties of nanocrystallite BFO as it can be seen from the subsequent observations. It was also shown that it is difficult to remove the secondary phase even by strong concentrated nitric acid leaching.

Figure 2b shows the small shifting of the strongest XRD peak due to the doping of BFO with Ni. The

main peak for the undoped bismuth ferrite is at about 32.12° (2θ) while for 5 mol% Ni-doped bismuth ferrite peak is at about 32.10°. The crystallite size of 5 mol% Ni doped bismuth ferrite is about 15.4 nm compared to the undoped perovskite bismuth ferrite which is about 14.7 nm. Atomic radius of Ni^{2+} (0.72 Å) is comparable with Fe^{3+} (0.64 Å) which may be the possible reason for doping of B site of ABO_3 perovskite (bismuth ferrite) with transitional metal ion. Due to the slight variation of atomic radius, strain will be generated in the matrix which may be the cause for slight reduction of crystallite size in Ni-doped sample.

3.2. Microstructural and elemental analysis

The synthesized powder is spread over a conducting carbon tape, and a field emission scanning electron microscope (FESEM) is used to observe the morphological details of the sample. Figure 3 shows the images of the BFO sample for both undoped and 5 mol% Ni-doped after annealing at 500 °C in air for 30 minutes at higher and lower resolutions.

For both undoped and Ni-doped sample, anisotropic growth with few interconnected pores among the agglomerated particulates is noted. Agglomerates have irregular polygonal to bimodal shape structures. Both samples exhibit strong agglomeration tendency among the granular particulates. Particle size for the undoped perovskite bismuth ferrite is about 20 nm while that for Ni-doped sample is found to be about 22 nm. The above results are closely connected to the experimental findings from our crystallite size measurement from XRD studies using Scherrer's formula. Hence, we confirmed that synthesis of the nanocrystalline undoped and Ni-doped bismuth ferrite with perovskite structure was performed successfully.

The chemical analysis of synthesized material was

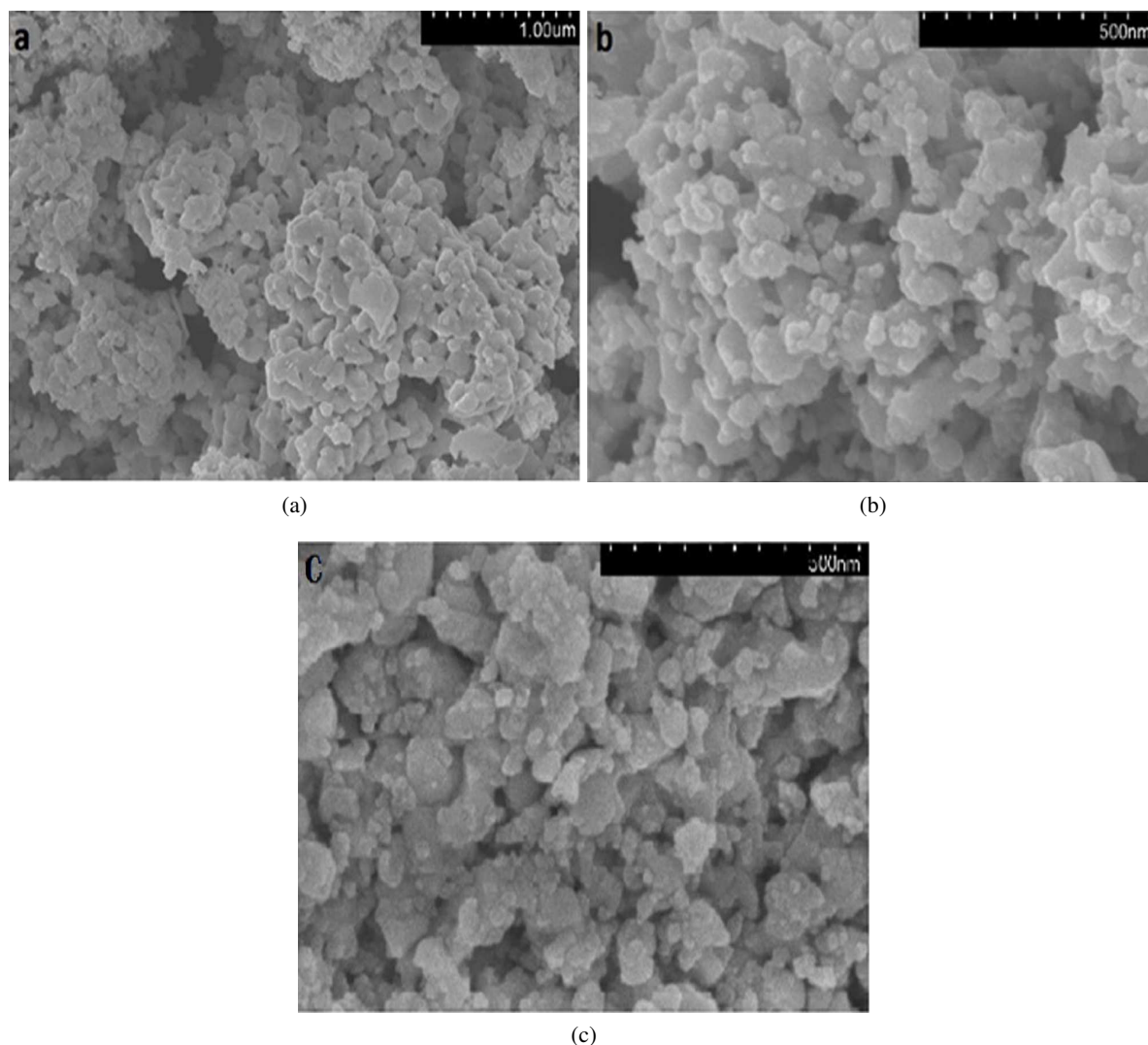


Figure 3. FESEM images of BFO doped with 5 mol% of Ni heat treated at 500 °C for 30 min (lower resolution (a) and higher resolution (b) images) and c) pure BFO powders heat treated at 500 °C for 30 min

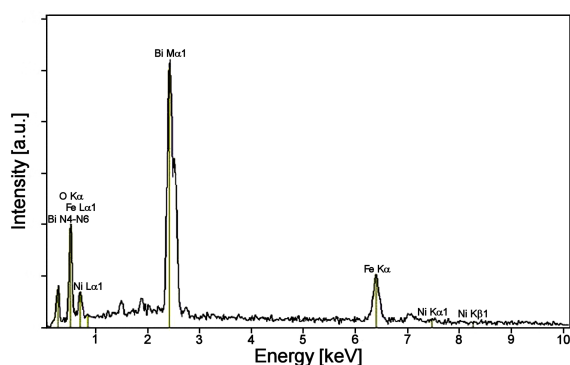


Figure 4. EDX plot of Ni-doped BFO sample heat treated at 500 °C for 30 min

obtained by EDX measurements. The EDX results (Fig. 4, Table 2) clearly confirm the presence of essential elements for the successful synthesis of the BFO-based material. Presence of Ni peak exhibits doping effect on the bismuth ferrite matrix which validates with corresponding experimental findings from X-ray diffraction study with shift in the peak towards left.

3.3. Dielectric properties

Figure 5 represents the variation of dielectric constant and loss tangent with frequency and Cole-Cole plot observed at room temperature for the undoped and 5 mol% doped pellets. The pellets with diameter of 10 mm and thickness of 1 mm were prepared with Ag paste coating on both sides, along with electrical wires, to erect the electrical connectivity for property measurements. The density of the undoped samples is found to be close to 96% of the theoretical density. Both dielectric constant and loss tangent exhibit similar nature of decreasing value with increase in frequency due to possible interfacial or space charge polarization phenomenon. The Cole-Cole plot predicts possible Maxwell-Wagner type interfacial polarization generated at the surface of nanocrystalline material. Dielectric constant of the undoped sample is about 100 at lower frequency range, whereas dielectric constant of 5 mol% Ni-doped bismuth ferrite is around 1100 almost (11 times higher than the value for the undoped material). It indicates high polarizability for Ni-doped sample since doping sup-

Table 2. Calculated crystallite size using Scherrer’s formula of powders heat treated under different conditions

Element line	Net counts	Net counts error	Amount [wt.%]
O K	1017	± 183	14.42
Fe K	1263	± 285	20.72
Ni K	86	± 102	4.83
Bi M	9163	± 609	60.03
Total			100.00

presses oxygen vacancy formation within the perovskite system.

With the increase in frequency the free motion of the charge carrier is due to space charge polarization resulting in characteristic variations in the curve for dielectric constant and loss tangent with frequency. The decrease of $\epsilon(\omega)$ with frequency can be explained as follows; at low frequencies the dielectric constant $\epsilon(\omega)$ for polar material arises due to the contribution of multicompo-

nent polarizability like deformational polarization (electronic and ionic polarization) and relaxation polarization (orientational and interfacial polarization) [18]. At higher frequencies, the dipoles will no longer be able to be on alignment with the applied external field, hence electron cloud oscillations begin to lag with the field. As the frequency is further increased, the dipole will be completely unable to follow the field and the orientation polarization stopped, so $\epsilon(\omega)$ decreases at higher

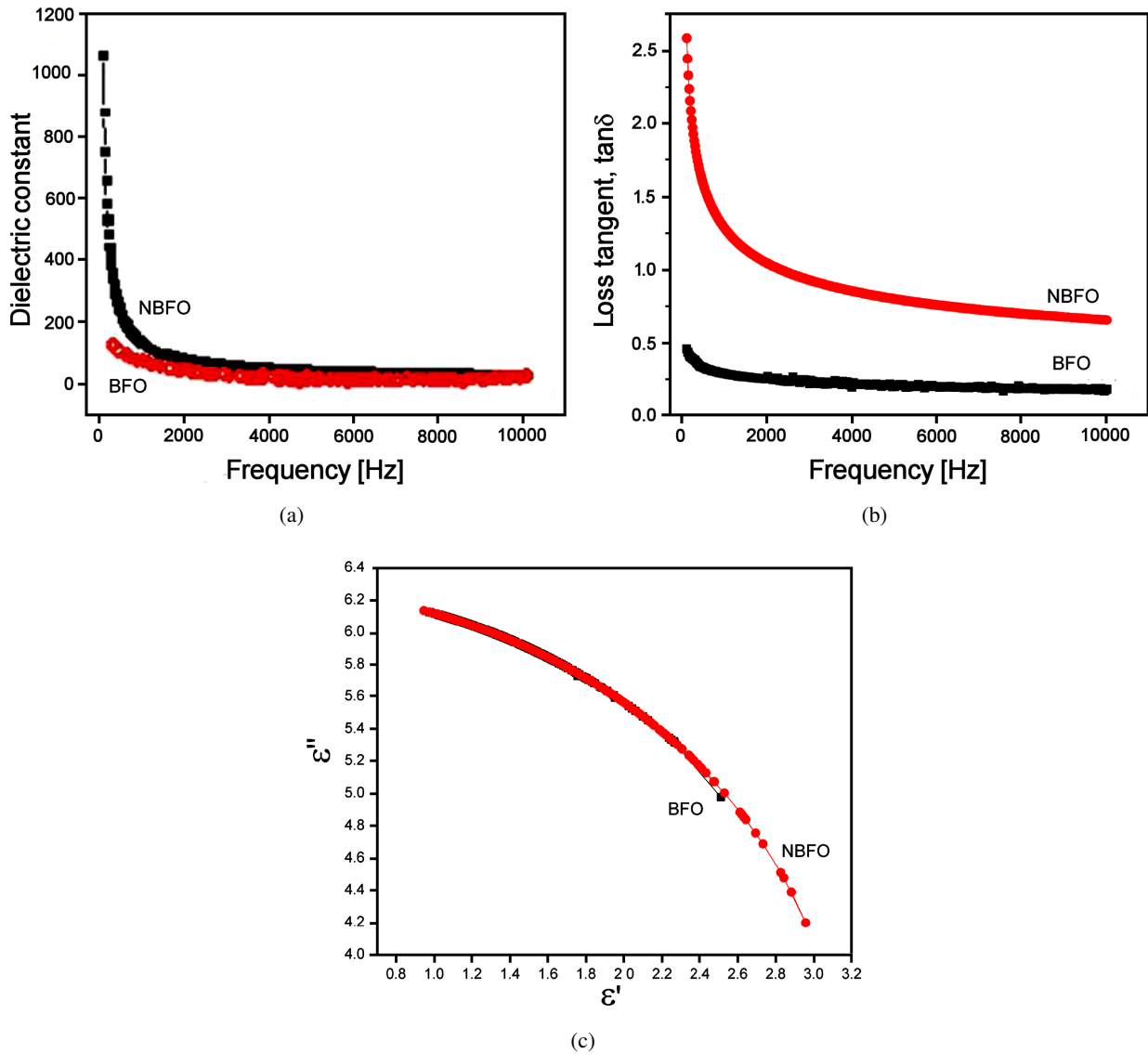


Figure 5. Undoped (BFO) and Ni-doped bismuth ferrite (NBFO) heat treated at 500 °C for 30 min: a) dielectric constant versus frequency curves, b) loss tangent ($\tan\delta$) versus frequency curves and c) Cole-Cole plot

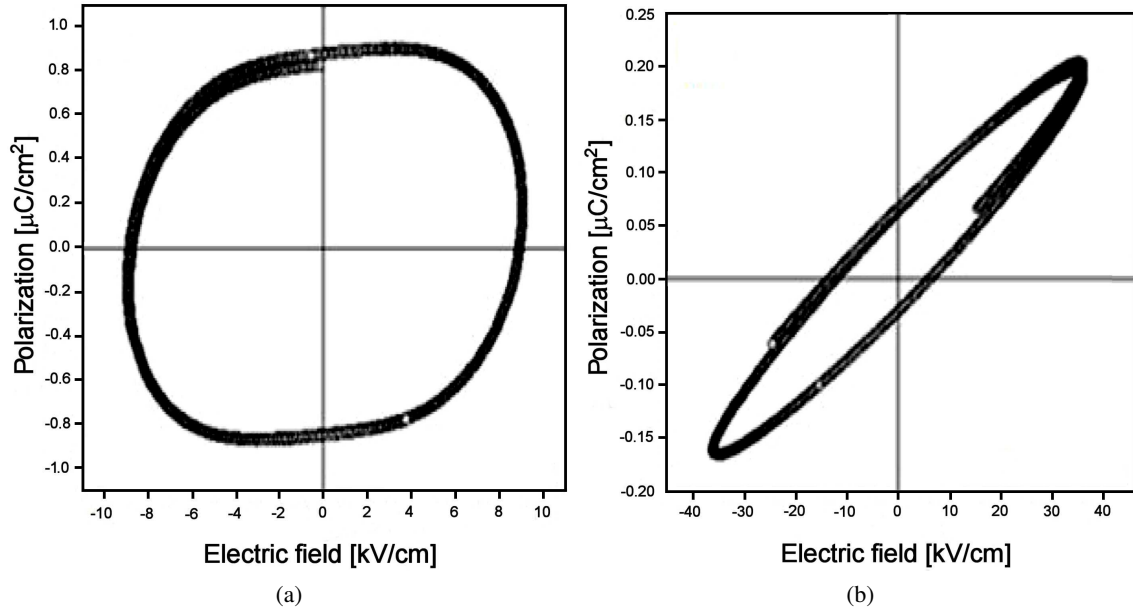


Figure 6. *P-E* hysteresis loops of: a) BFO and b) Ni-doped BFO samples heat treated at 500 °C for 30 min

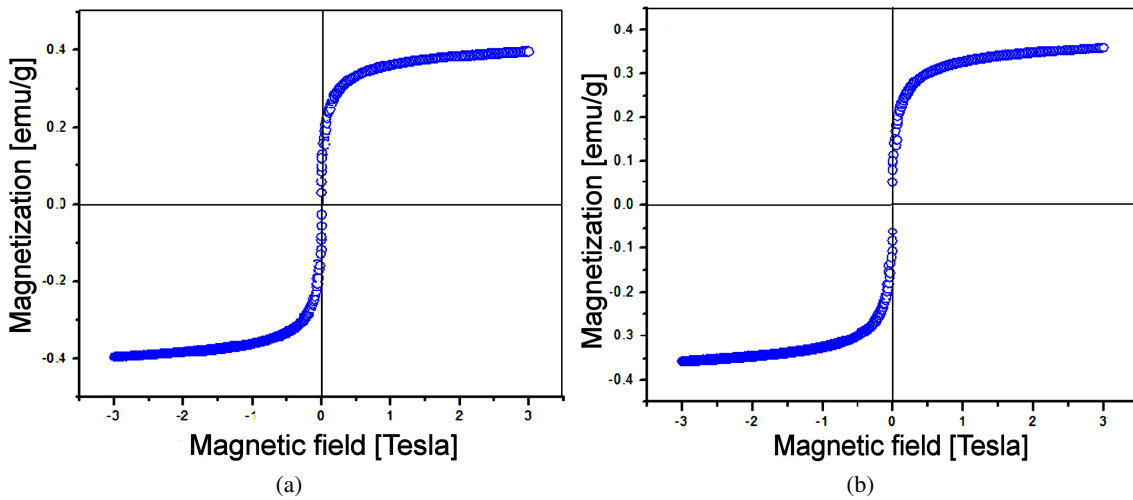


Figure 7. Magnetization versus magnetic field hysteresis of: a) BFO and b) Ni-doped BFO samples heat treated at 500 °C for 30 min

frequencies approaching a constant value due to the interfacial or space charge polarization only. The Cole-Cole plot justifies the contribution of grain boundary polarization since the system component has nano dimension particulates and it arises due to possible Maxwell-Wagner type interfacial polarization at the grain boundary of the nanocrystalline material.

3.4. Ferroelectric properties

Pellets (diameter of 10 mm and thickness of 1 mm) with Ag paste on both sides were prepared after heating at 500 °C for 30 minutes and used for ferroelectric study performed at 200 Hz. For the undoped sample, saturation polarization and remnant polarization could not be determined correctly since material behaviour is not ferroelectric in nature. The sample is observed to

exhibit conducting nature as evident from the character of the *P-E* loop analysis (Fig. 6). The conducting nature arises due to possible leakage current in nanocrystalline bismuth ferrite due to oxygen deficiency in the perovskite structure. Thus, doping effect is once again confirmed from ferroelectric loop studies since addition of Ni²⁺ leads to suppression of oxygen vacancy leading to lowering conductivity in the sample and polarization arises contributing towards better ferroelectricity in the doped sample. Enhanced ferroelectricity observed may be due to increase in drastic change in dielectric constant or polarizability of the sample after Ni-doping. For the undoped sample, area under the *P-E* loop is more than that for Ni-doped sample. Saturation polarization (P_s) obtained for Ni-doped sample is found to be 0.209 $\mu\text{C}/\text{cm}^2$, remnant polarization (P_r) 0.074 $\mu\text{C}/\text{cm}^2$

and coercive field is 7.45 kV/cm. Breakdown voltage for the undoped sample is 10 kV/cm, while for Ni-doped sample it is 40 kV/cm.

3.5. Magnetic properties

The magnetization curve of the undoped nanocrystalline BFO sample clearly exhibits saturation at higher magnetic field. This happens due to the enhanced surface spin contribution in comparison to the bulk perovskite ferrite. Crystallite size obtained from XRD for the undoped BFO is about 14.7 nm which is substantially lower than the spin cycloid structural arrangement of about 62 nm in dimension. Such spin cycloidal is mostly responsible for antiferromagnetic nature in bulk bismuth ferrite while in the present case nanocrystalline BFO has lower dimension results in breaking of such distorted magnetic structure leading to super paramagnetic and ferromagnetic nature in the sample. The undoped nanocrystalline bismuth ferrite exhibits nearly zero coercive field. From $M-H$ curve analysis remanent magnetization (M_r) is measured around 0.124 emu/g at zero external applied field and saturation magnetization (M_s) of about 0.3961 emu/g. Squareness ratio (M_r/M_s) is about 0.3130. Similarly for Ni-doped nanocrystalline BFO zero coercive field is noted which corresponds to perfect super paramagnetic and strong ferromagnetic nature. Since we observed that crystallite size of Ni-doped BFO is slightly higher than for the undoped BFO, hence the extent of breakdown of spin-cycloidal magnetic moment shows less value, which may cause slight lowering of magnetic saturation value.

For Ni-doped BFO sample, the saturation magnetization decreases due to substitution of Fe^{3+} by Ni^{2+} having lower magnetic moment than Fe. Strong ferromagnetic property has been identified in Ni-doped BFO with a remanent magnetization (M_r) of 0.1 emu/g, and zero coercive field (H_c). Saturation magnetization (M_s) is about 0.3573 emu/g and the squareness ratio obtained is (M_r/M_s) 0.2798. Thus the squareness ratio is found to be slightly lower for Ni-doped nanocrystalline BFO in comparison to nanocrystalline undoped BFO.

IV. Conclusions

Chemical route can be used to synthesize nanocrystalline undoped and Ni-doped bismuth ferrite with perovskite structure and crystallite size of about 14.7 and 15.4 nm, respectively. Rise in doping concentration leads to generation of secondary phase, thus dopant concentration is maintained to 5 mol%. Morphological analyses exhibits irregular polygonal to bimodal shape agglomerates with few interconnected pores. Dielectric constant for the undoped bismuth ferrite is about 100, while for 5 mol% Ni doped sample it is noted around 1100 (at low frequency). Such drastic change leads to higher polarizability which also enhances ferroelectricity with Ni doping on perovskite bismuth ferrite. Both nanocrystalline and Ni-doped BFO exhibits super paramagnetic nature due to suppression of spin cycloid mag-

netic moment. Saturation magnetization of Ni-doped is slightly lower than for undoped BFO due to smaller crystallite size.

Acknowledgement: Authors would like to thank DST Nanmission and UGC-UPE for giving infrastructural supports and P.G fellowship in this programme.

References

1. P. Borisov, A. Hochstrat, X. Chen, W. Kleemann, C. Binek, "Magnetoelectric switching of exchange bias", *Phys. Rev. Lett.*, **94** [11] (2005) 117203-4.
2. X. Martí, F. Sánchez, J. Fontcuberta, M.V. Cuenva-García, C. Ferrater, M. Varela, "Exchange bias between magnetoelectric YMnO_3 and ferromagnetic SrRuO_3 epitaxial films", *J. Appl. Phys.*, **99** [08P302] (2006) 1–3.
3. J. Dho, X. Qi, H. Kim, J.L. Driscoll-MacManus, M.G. Blamire, "Large electric polarization and exchange bias in multiferroic BiFeO_3 ", *J. Adv. Mater.*, **18** [11] (2006) 1445–1448.
4. V. Laukhin, V. Skumryev, X. Martí, D. Hrabovsky, F. Sánchez, M.V. Cuenva-García, C. Ferrater, M. Varela, U. Lüders, J.F. Bobo, J. Fontcuberta, "Electric-field control of exchange bias in multiferroic epitaxial heterostructures", *Phys. Rev. Lett.*, **97** [22] (2006) 227201-4.
5. H. Béa, M. Bibes, F. Ott, B. Dupé, H.X. Zhu, S. Petit, S. Fusil, C. Deranlot, K. Bouzehouane, A. Barthélémy, "Mechanisms of exchange bias with multiferroic BiFeO_3 thin films", *Phys. Rev. Lett.*, **100** [1] (2008) 0172041-4.
6. C. Michel, J.M. Moreau, G.D. Acheubach, R. Gerson, W.J. James, "The atomic structure of BiFeO_3 ", *Solid State Commun.*, **7** [9] (1969) 701–704.
7. P. Fischer, M. Polomska, I. Sosnowska, M. Szymanski, "Temperature dependence of the crystal and magnetic structures of BiFeO_3 ", *J. Phys. C. Solid State.*, **13** [10] (1980) 1931–1940.
8. G.A. Smolenskii, I.E. Chupis, "Ferroelectromagnets", *Sov. Phys. Uspekhi.*, **25** [7] (1982) 475–493.
9. Yu.F. Popov, A.K. Zvezdin, G.P. Vorob'ev, A.M. Kadomtseva, V.A. Murashev, D.N. Rakov, "Linear magnetoelectric effect and phase-transitions in bismuth ferrite, BiFeO_3 ", *JETP Lett.*, **57** (1993) 69–73.
10. I. Sosnowska, T. Peterlin Neumaier, E. Streichele, "Spiral magnetic ordering in bismuth ferrite", *J. Phys. C. Solid State.*, **15** [23] (1982) 4835–4846.
11. K. Ueda, H. Tabata, T. Kawai, "Coexistence of ferroelectricity and ferromagnetism in BiFeO_3 - BiTiO_3 thin films at room temperature", *Appl. Phys. Lett.*, **75** [4] (1999) 555–557.
12. V.R. Palkar, K. Ganesh Kumara, S.K. Malik, "Observation of room-temperature magnetoelectric coupling in pulsed-laser-deposited $\text{Bi}_{0.6}\text{Tb}_{0.3}\text{La}_{0.1}\text{FeO}_3$ thin films", *Appl. Phys. Lett.*, **84** [15] (2004) 2856–2858.

13. Y.K. Jun, W.T. Moon, C.M. Chang, H.S. Kim, H.S. Ryu, J.W. Kim, K.H. Kim, S.H. Hong, “Effect of Nb-doping on electric and magnetic properties in multiferroic BiFeO₃ ceramics”, *Solid State Commun.*, **135** [1-2] (2005) 133–137.
14. Y.H. Lee, J.M. Wu, C.H. Lai, “Effect of La doping in multiferroic properties of BiFeO₃ thin films”, *Appl. Phys. Lett.*, **88** [4] (2006) 0429031-3.
15. J.K. Kim, S.S. Kim, W.J. Kim, A.S. Bhalla, R. Guo, “Enhanced ferroelectric properties of Cr-doped thin films grown by chemical solution deposition”, *Appl. Phys. Lett.*, **88** (2006) 132901-3.
16. A. Maitre, M. Francois, J.C. Gachon, “Experimental study of the Bi₂O₃-Fe₂O₃ pseudo-binary system”, *J. Phase. Equilib. Diff.*, **25** [1] (2004) 59–67.
17. G. Biasotto, A.Z. Simões, C.R. Foschini, S.G. Antônio, M.A. Zaghete, J.A. Varela, “A novel synthesis of perovskite bismuth ferrite nanoparticles”, *Process. Appl. Ceram.*, **5** [3] (2011) 171–179.
18. D.W. Kingery, H.K. Bowen, D.R. Uhlmann, *Introduction to Ceramics*, 2nd edition, Wiley-InterScience Publications, Canada, 1976.